Clin Exp Metastasis (2011) 28:779–791
DOI 10.1007/s10585-011-9409-5

RESEARCH PAPER

Tumor–stromal interactions of the bone microenvironment: in vitro findings and potential in vivo relevance in metastatic lung cancer models

Diego Luis-Ravelo · Iker Antón · Silvestre Vicent · Igor Hernández · Karmele Valencia · Carolina Zandueta · Susana Martínez-Canarias · Alfonso Gúrpide · Fernando Lecanda

Received: 8 November 2010 / Accepted: 11 July 2011 / Published online: 28 July 2011

Abstract Lung cancer comprises a large variety of histological subtypes with a frequent proclivity to form bone metastasis; a condition associated with dismal prognosis. To identify common mechanisms in the development of osteolytic metastasis, we systematically screened a battery of lung cancer cell lines and developed three models of non-small cell lung cancer (NSCLC) with a common proclivity to form osseous lesions, which represented different histological subtypes. Comparative analysis revealed different incidences and latency times. These differences were correlated with cell-type-specific secretion of osteoclastogenic factors, including macrophage inflammatory protein-1α, interleukin-8 and parathyroid hormone-related protein, some of which were exacerbated in conditions that mimicked tumor–stroma interactions. In addition, a distinct signature of matrix metalloproteinase (MMP) activity derived from reciprocal tumor–stroma interactions was detected for each tumor cell line. Thus, these results suggest subtle differences in the mechanisms of bone colonization for each lung cancer subtype, but share, although each to a different degree, dual MMP and osteoclastogenic activities that are differentially enhanced upon tumor–stromal interactions.

Keywords Osteolytic · Microenvironment · MMPs · Cachexia · Osteoclast

Abbreviations

i.c.	Intracardiac
SCDC	Single cell derived colonies
TRAP	Tartrate-resistant acid phosphatase
qPCR	Real time quantitative RT-PCR
MMP	Metalloprotease
CM	Conditioned medium
NSCLC	Non-small cell lung cancer
SCLC	Small-cell lung cancer

Introduction

Lung cancer presents the highest cancer mortality in western countries with a 5-year survival rate lower than 10–15% [1]. Non-small cell lung cancer (NSCLC) represents the largest subgroup of patients and accounts for ~75% of all cases. This subset includes different subtypes such as adenocarcinoma (30–40%), squamous cell carcinoma (20–25%), and large cell carcinoma (15–20%) [2]. NSCLC also includes carcinoid tumors (1–5%), which display neuroendocrine features with close similarity to the subset of small cell lung cancer (SCLC) [3], the other

D. Luis-Ravelo, I. Antón and S. Vicent have contributed equally to this work.

Electronic supplementary material The online version of this article (doi:10.1007/s10585-011-9409-5) contains supplementary material, which is available to authorized users.

D. Luis-Ravelo · I. Antón · S. Vicent · I. Hernández · K. Valencia · C. Zandueta · S. Martínez-Canarias · F. Lecanda (✉)
Division of Oncology, Adhesion and Metastasis Laboratory, Center for Applied Medical Research (CIMA), University of Navarra, 31080 Pamplona, Spain
e-mail: flecanda@unav.es

Present Address:
S. Vicent
Division of Hematology/Oncology, Department of Pediatrics, Stanford University, Stanford, CA, USA

A. Gúrpide
Department of Oncology, Clínica Universidad de Navarra (CUN), University of Navarra, Pamplona, Spain

subgroup of tumors. Besides their different histology, both entities display a common ability to metastasize locally to the thoracic cavity and to distant sites including the skeleton [3]. Bone tropism occurs in 40% of patients with NSCLC and is clinically associated with pain, paraneoplastic syndromes, marrow compression, and fractures [4]. This reduction in quality of life is often associated with dramatic decline in survival (<6 months) and expensive clinical management [5].

Tumor cell metastasis is a multistep process that requires the coordinated action of several pathways that drive invasion and intravasation, evasion of inmunosurveillance, arrest, extravasation, and distant outgrowth [6, 7]. All of these steps are highly influenced by the interaction of tumor cells with the surrounding microenvironment, which modulates their invasion and colonization of the target tissue. The importance of tumor–stromal interactions in bone metastasis has been shown in models of breast [8] and renal cell [9] carcinoma, in which osteoclastic activity is stimulated by tumor-secreted factors. This activity is exacerbated by transforming growth factor (TGF-β) release in the microenvironment by osteoclast resorption, which creates a perpetuated "vicious cycle" [10, 11]. Recently, in a model of NSCLC, aggressive bone colonization was mechanistically driven by a similar osteoclastic activity fuelled by stroma-derived TGF-β [12]. Complementary to this, aggressive bone matrix degradation is also mediated by tumor-released metalloproteolytic activity that is enhanced by tumor–stroma interactions. All different subtypes of NSCLC share a common proclivity to form bone metastasis. Given the common poor survival rate of bone metastasis patients despite their diverse histopathological and clinical course, the question about shared mechanisms of bone metastasis remains unexplored. Thus, appropriate experimental models are required to establish better the pattern and spectrum of osseous lesions observed in humans. This information could be relevant in the search for critical factors that are involved in this process, and to test novel therapeutics rigorously.

At present, several models of lung cancer metastasis have been developed [13–17]. Orthotopic lung cancer models in nude mice by intrapulmonary injection or by surgical implantation lead to development of local lesions [14, 18] or metastatic spread to nearby or distant sites [19]. Recently, some genetic models of lung adenocarcinoma with metastatic spread have also been described [20, 21]. However, to date, the limited number of lung cancer models with osseous metastasis, given the heterogeneity of lung cancer subtypes, has hampered the study of the mechanisms by which key molecular targets can be identified. These models will help to elucidate common and specific differences in the mechanisms of bone homing and colonization.

In this study, we developed different models of lung cancer metastasis of different histological subtypes. Comparison of these models revealed different patterns of bone colonization and cachexia development. Our data suggest an association between tumor–stromal interactions in vitro that contribute to different degrees of matrix metalloproteinase (MMP) and osteoclastogenic activities and the severity and progression of osseous metastatic lesions.

Materials and methods

Cell culture

SCLC (NCI-H69, -H82, -H187, -H345, -H446 and -H510) and NSCLC cell lines (NCI-H358, -H1385, -H1299, -H441, -H661, -H676, -H2087, -H460, A549, SK-MES-1, H720 and H727) were a kind gift of A. Gazdar (University of Texas Southwestern, Dallas, TX). The NCI-H460 isolated from a pleural effusion [22], from a patient with a human large cell carcinoma with mutant k-Ras and wild-type TP53 [23, 24]. A549 cell line was originally obtained from a IIIA stage mixed adenocarcinoma. H727 cell line was isolated from a IIIA stage carcinoid tumor, from a lung biopsy. Murine stromal ST-2 was a kind gift from Dr. Civitelli (Washington University, St. Louis, MO). This bone marrow-derived cell line was used to mimic tumor–stromal interactions as they are capable of induce osteoblastic phenotype. All cultures and cocultures were maintained in RPMI 1640 medium supplemented with 10% fetal bovine serum, 50 U/ml penicillin, and 50 μg/ml streptomycin in a humidified atmosphere of 5% CO_2 in air at 37°C.

Gene expression analysis

Qualitative RT-PCR was performed for screening in all lung cancer cell lines on PTC-100 Thermo Cycler (MJ Research Inc, MA, USA). PCR conditions and sequence of primers can be found in supplementary material.

Real-time quantitative PCR was performed using a Gene Amp 7300 sequence detection system (Applied Biosystems) according to manufacturer's recommendations. Mouse and human specific primers (500 nM) for MMP-2, -3, -9 and -10 were used. Reactions were performed in SYBR Green PCR Master Mix (Applied Biosystems). As endogenous control, specific mouse or human GAPDH were used. The mean cycle threshold value (Ct) from triplicate samples was used to calculate gene expression. The expression is represented as the fold increase relative to each tumor cell alone (tumor MMP expression) or ST-2 alone (stroma MMP expression) and was determined by the

comparative Ct method (ΔΔCt). Experiment was repeated three times with identical results.

Coculture conditions

ST2 (0.5×10^5), tumor cells (10^6) or both were seeded in 10 cm culture dishes. For coculture, one or two million tumor cells were seeded with 5×10^5 murine ST2 cells for 2 days. Conditioned media from ST2 single culture or from cocultures were collected before extracting RNA and added at 50% (v/v) dilution with fresh medium to tumor cells for 2 days. Twenty-four hours later fresh conditioned medium was added again for one more day until RNA extraction was extracted.

Chemotaxis assay

Chemotaxis assay was performed on commercial cell culture invasion inserts with 8-μm pore size polycarbonate membrane (QCM™ 96-well cell chemotaxis assay, Chemicon International). The assay was started by adding 50,000 cells in 100 μl of 0,4% FCS-DMEM on the upper chamber and 120 μl of 10% FCS-DMEM in the lower chamber as a chemoattractant to induce migration. Cells were incubated for 6 h at 37°C and 5% CO_2, and the insert membranes were then prepared according to manufacturer's recommendations. Cells were dislodged with Cell Detachment Solution from the underside and stained using CyQuant GR Dye®. Fluorescence was determined using 480/520 nm filter set. Experiment was repeated three times, and each condition was done in sixplicate as described previously [25].

Osteoclast differentiation

Non-adherent bone marrow mononuclear cells were isolated from femurs and tibias of 3- to 6-week-old wild-type C57BL/6 (Harlan Iberica, Spain). Cells were cultured on 100 mm dishes overnight in α-MEM (Invitrogen) media supplemented with 10% fetal bovine serum (Gibco), and penicillin/streptomycin (Gibco). Non-adherent bone marrow mononuclear cells were collected and erythrocytes were lysated with Red Blood Cell Lysis Buffer (Bioscience) (5 min. at 37°C). Cells were seeded in 48 Well Plates at 2×10^6 cells/ml per well, were grown for 24 h on α-MEM supplemented in the presence of 20 ng/ml recombinant mouse M-CSF (R&D Systems) and of 40 ng/ml human sRANKL (Peprotech) to generate osteoclast precursors (hereafter also called BMM). Conditioned media were added to BMMs for 6 days and subsequently the cells were subjected to TRAP staining (Sigma, St. Louis, MO), according to the manufacturer's instructions.

Global MMP activity

Single cell cultures or cocultures were washed with PBS and serum starved for 24 h. The conditioned media and medium-only (control) were concentrated using a 5 kDa cutoff Amicon concentrator (Millipore). Global MMP activity was measured in supernatants using an assay based on the cleavage of synthetic fluorogenic peptides. Substrate 1 (Bachem M-2110) was preferentially cleaved by MMP-3, and -9 and substrate 2 (R&D systems, Minneapolis, MN, USA) was preferentially cleaved by MMP-3 and -10. Supernatants were incubated at 25× with the fluorogenic peptides at a final concentration of 20 μM (2 h at 37°C). GM6001 was used as global MMP inhibitor at 100 μM. Fluorescence measurement was kinetically performed on fluorescence spectrometer (excitation 320 nm, emission 405 nm, Spectra MAX GeminiXS, Molecular Devices, Sunnyvale, CA, USA). The slope was calculated over the linear range using 16 different time points for each condition. Experiments were repeated three times with identical results.

Animals and intracardiac injection (i.c.)

Female athymic nude mice (Harlan Iberica, Spain) were maintained under specific pathogen-free conditions. For i.c., cells were seeded a day before injection at 50% confluence. Cells were gently washed with PBS, detached, and resuspended at 2×10^6 cells/ml in sterile PBS. Suspensions had to show ≥95% cell viabilty. Mice ($n = 8$ each group) were anaesthetized with ketamine (100 mg/kg body weight) and xylazine (10 mg/kg of body weight) before injection. One hundred microliters containing 2×10^5 cells were injected into the left cardiac ventricle of the 4-week old mice (Harlan Iberica, Spain) using a 29-G needle syringe. All the animals were sacrificed according to the approved protocols of the Local Animal Committee (University of Navarra, protocol 003-04).

Radiographic, microcomputed tomographic (μCT) analysis and bioluminescence imaging

X-ray radiography was performed under anaesthesia, with mice place on the prone position on sensitive radiographic film (MIN-R, Eastman Kodak). The mice were exposed to X-irradiation at 20 kV for 20 s using a Faxitron instrument (Faxitron, Buffalo Grove, IL, USA). The area of osteolytic metastasis was assessed with a computerized image analysis system, AnalySIS® (soft imaging system GmbH, Münster, Germany). High resolution X-ray film scans with 2× magnification were captured at 1200 ppi using a Epson Expression 1680 Pro scanner (Long Beach, CA, USA). Quantification of metastatic area was performed twice after

calibration, by two independent observers. For Kaplan–Meier curves metastasis was scored as the time to first appearance of a signs of cachexia and difficulty to walk.

Whole femoro-tibial joints were analyzed by a μCT system (micro CAT^{TM} II, Siemens Preclinical Solutions, Knoxville, TN, USA) at 75.0 kVp and 250.0 μA. The scans were performed at 10 μm resolution. 2D CT images were reconstructed using a standard convolution-back projection procedure with a Shepp-Logan filter. Images were stored in 3D arrays with a voxel size of 19 μm × 19 μm × 23 μm.

For bioluminescence imaging and analysis, mice were anaesthetized and injected intraperitoneally with 1.5 mg of D-luciferin in 100 μl of PBS. Imaging was completed at 2 min exactly for each group of mice with a Xenogen IVIS system coupled to Living Image acquisition and analysis software (Xenogen Inc.). Photon flux was calculated for each mouse by using a circular region of interest for each hind limb. Background value (from luciferin-injected mouse with no tumor cells) was subtracted from each measurement.

Isolation of single cell-derived colonies (SCDC) from long bones

Mice were sacrificed according to the approved protocols of the Local Animal Committee (University of Navarra, protocol 003-04). Cells previously transduced with luciferase-bearing plasmid containing neomycin resistance gene were isolated from bone marrow of lower limbs. Long bones were excised, and cleaned of all soft tissues. Marrow cells were released by "flushing", introducing 5–10 ml of RPMI medium containing 2× penicillin/streptomycin with a 27 gauge needle in the distal epiphysis through the bone marrow compartment. Cell clumps were disaggregated by passing medium containing cells through 27 G needle syringe. Cells were plated in 10 or 15 cm dishes expanded for 5 days in medium containing 0.4 mg/ml G-418. This procedure was performed separately for each femur and tibia of 7 mice per group. SCDCs were counted under light microscope after crystal violet staining.

Local tumor growth

Cells (10^6 cells/100 ml PBS) were inoculated into the thigh of female nude mice. Tumor volume was measured every three days with a digital calliper and calculated as previously described [10].

Statistical analysis

Log-rank test was used to calculate the statistical significance (P value) of differences observed among Kaplan–Meier curves. Chemotaxis assay was analyzed using Student t test. Cell cycling time and subcutaneous tumors were analyzed by Welch test followed by Tamhane multiple comparison test. To study differences between bone metastatic cells in migration, body weight and number of osteoclasts, data were analyzed by ANOVA followed by Tukey multiple comparison test. Non-parametric data were analyzed by Kruskal–Wallis test with Dunn's multiple comparison test (metastatic area) or Bonferroni's adjust (MMP activity and expression). Values were expressed as means ± SD (parametric) or means ± SEM (non-parametric) and statistical significance was defined as $P < 0.05$ (*), $P < 0.01$ (**), and $P < 0.001$ (***).

Results

In vitro strategy to select potential bone metastatic lung cancer cell lines

We screened a panel of human lung cancer cell lines by semi-quantitative RT-PCR. Based on previous findings, we assessed the expression of several genes related to tumor progression and metastasis in other models. *MMP-2* cleaves collagen type IV and is involved in invasiveness and tumor metastasis in different organs [26, 27]; galectin-3 (*LGALS3*) promotes metastasis by acting on localization of transendothelial mediators [28]; macrophage inflammatory protein (*MIP-1-α*) and parathyroid hormone-related protein (*PTHrP*) are osteoclastogenic factors that are involved in osteolytic metastasis [29–31]; *CTGF* was identified as a bone metastasis virulence gene in highly bone metastatic subpopulations of breast cancer cells [32]; and osteopontin (*SPP1*), which promotes osteoclast adhesion to bone [33]. As shown in Fig. 1a, we found heterogeneous expression for each gene in different cell lines, with expression of some genes in NSCLC that were absent in SCLC. NSCLC cell lines SK-MES-1, A549, H460, H1299 and H727 showed strong signals in at least five genes. The relative expression of these genes in tumor versus normal lung epithelial cells can be found in supplementary Fig. 1. These findings, together with the higher incidence of NSCLC in humans, led us to focus on NSCLC.

We performed a chemotaxis assay in NSCLC cell lines. Cell migration to the lower chamber using 10% FBS was quantified by fluorescent labeling in a Boyden chamber assay. As illustrated in Fig. 1b, several cell lines showed overt migration towards the lower compartment, including A549, H1299, H460, SK-MES-1 and H727, while others did not exhibit this phenotype.

The five lung cancer cell lines that fulfilled both variables, migratory and gene expression patterns, were subsequently used to test their metastatic ability in vivo.

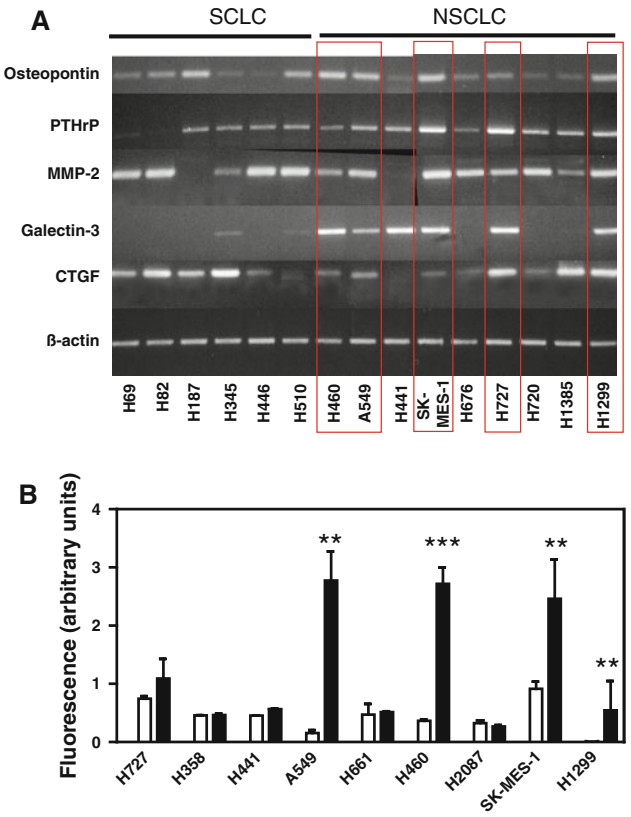

Fig. 1 **a** Screening by RT-PCR of a panel of lung cancer cell lines of small (SCLC) and non-small cell lung cancer (NSCLC). Genes implicated in metastasis in other models, including osteopontin, PTHrP, MMP-2, galectin-3, and CTGF, were compared to a housekeeping gene, *β*-actin. Cell lines expressing all of these genes are highlighted in *red*. **b** Chemotaxis Assay. Cells were uninduced (*open square*) or induced (*filled square*) by 10% serum in the lower compartment of Boyden chambers for 6 h. Cells migrating to the lower compartment were labeled with a fluorescent dye. Total fluorescence was measured using 480/520 nm filter set. Student *t* test (**$P < 0.01$; ***$P < 0.001$)

In vivo assessment of bone metastasis

To investigate the ability of selected cell lines to metastasize to bone, we used a murine model that recapitulated late steps of metastasis such as organ homing and colonization. After intracardiac inoculation (i.c.) of luciferase-transfected cells, animals were monitored for signs of disease (cachexia, paralysis, or kyphosis). Animals inoculated with different cell lines displayed distinct times of incidence and global survival, which indicated different metastatic activity (Fig. 2a). Despite common expression of previously selected genes, development of metastasis was different for each cell line with respect to tissue specificity. Of all five cell lines tested, only A549 (adenocarcinoma), H460 (large cell carcinoma), and H727 cells (carcinoid) thrived with high specificity in bone (Fig. 2b; Table 1). H460 cells were detected by bioluminescence in the hind limbs in 3/8 animals 3 weeks after i.c. inoculation. In H727 cells, 7/8 animals displayed bioluminescence in sites compatible with an osseous location, including hind limbs and the spine at 6 weeks after xenografting (Fig. 2b). A549 cells produced significant metastatic lesions in long bones in 3/8 animals 3 weeks after i.c. inoculation, and vertebrae, where mixed osteolytic lesions and periosteal new bone formation were observed by X-ray examination and histology (Fig. 2c and supplementary Fig. 2). Indeed, some animals showed a dramatic reduction of limb motility, which suggested spinal cord infiltration. Metastases in other organs were confined to a lesser extent in these models (Fig. 2d, top left; Table 1). In contrast, other cell lines showed a preference for the lungs, such as SK-MES-1 (Fig. 2b, d, top right panel). Indeed, histological examination showed SK-MES-1 lung metastatic cells in the lung parenchyma of 2/8 mice, whereas H1299 cells were frequently found in the nasal and mandibular bones (Fig. 2b, d, bottom). Finally, inoculated animals displayed axillar and cervical lymph node metastasis in H727 injected mice, and metastasis in axillar and brachial lymph nodes, in SK-MES-1 injected animals (Table 1).

Kaplan–Meier curves that monitored bone-metastasis-free survival showed shorter latency time in animals inoculated with A549 and H460 cells compared to H727 cells, in which bone metastasis developed more slowly (Fig. 2e). These results indicate that the three cell lines displayed a preferential bone metastatic location. Differential incidences and latency times could involve different mechanism of bone metastasis.

Bone imaging analysis

Macroscopic osteolytic lesions of all three cell lines were found in the hindlimbs in the proximal tibial and distal femoral regions in the primary spongiosa, and in some cases, in the cortical bone, arising from the periosteum. Lesions induced by H460 and A549 cells appeared in distal femoral and proximal tibial metaphyses, in the primary spongiosa, and with low frequency in the epiphysis. In addition to these sites, H727 cells showed a marked epiphyseal location (Fig. 3a). At the tumor–bone interface between the bone marrow and the endosteal surface of the diaphysis, a number of multinucleated TRAP-positive osteoclasts per bone area were evident for all three cell lines (Fig. 3a, right panel).

Tumor burden

We determined whether tumor burden correlated with the degree of osteolytic lesions. After i.c. inoculation, we assessed the metastatic area by X-ray imaging and counted the number of isolated cell clones after marrow "flushing"

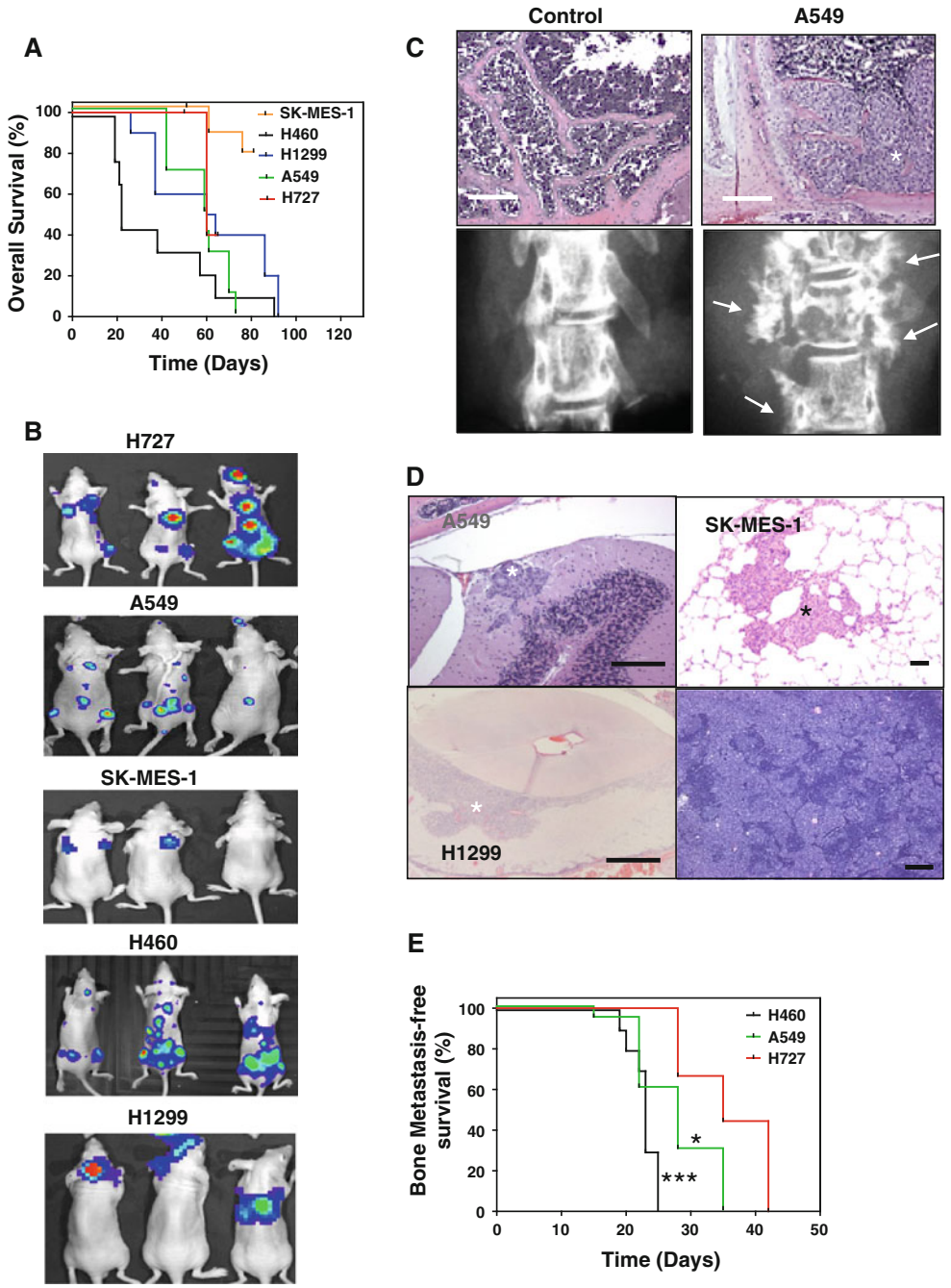

Fig. 2 **a** Kaplan–Meier survival curves of mice inoculated in the left ventricle with H460, H1299, SK-MES-1, H727, or A549 cells ($n = 8$ each group). **b** In vivo bioluminescence imaging of athymic nude mice visualized 2 weeks (H460 and A549 cells) and 6 weeks postinoculation (H1299, H727 and SK-MES-1). Different times were needed because of different latency time. Representative images of mice groups are shown in "**c**". *Top*: Histological examination of spinal metastasis induced by A549 cells ("*" indicates metastatic cells). *Bar* 250 μm. *Bottom*: X-ray imaging of mixed osteolytic lesions and new bone formation induced in vertebra by A549 cells (*arrows*). **d** Histological examination of metastatic cells in other organs. *Top left panel*: Cerebellar metastasis induced by A549 cells. *Bottom left panel*: Mandibular metastasis derived from H1299 cells. *Left bars* 200 μm. *Top right panel*: Lung metastasis in SK-MES-1 inoculated mice. *Top right bar* 100 μm. *Bottom-right panel*: tumor cells in a lymph node. *Bar* 200 μm. "*" denotes the presence of tumor cells. **e** Kaplan–Meier curve of bone metastasis-free survival in three cell lines thriving in the osseous compartment. Differences in latency time were observed between H727 and the other two cell lines (Log-rank test, $*P < 0.05$ A549 vs. H727; $***P < 0.001$ H460 vs. H727)

in H460, A549 and H727 cells. A549-inoculated mice developed large bone lesions in 29 days, and an average of 2225 single cell derived colonies (SCDCs) were isolated and counted from flushed bones. In contrast, H727 showed prominent overt metastasis at 59 days post-inoculation, but the number of isolated SCDCs in a group of eight animals

Table 1 Site and incidence of metastasis of luciferase (LUC) transfected of H460, H727, A549, H1299 and SK-MES-1

Cell line	Mice with bone mets at 21 days	Site of metastasis at sacrifice[a]										
		Hindlimbs	Spine	Lung	Lymph Nodes	Gingival	Brain	Kidney	Adrenal gland	Retro-orbital region	Cachexia	Paralysis
H460-LUC	3/8 (38%)	7/8 (88%)		1/8 (13%)							3/8 (38%)	2/8 (25%)
A549-LUC	3/8 (38%)	7/8 (88%)	3/8 (38%)	1/8 (13%)		1/8 (13%)	1/8 (13%)	1/8 (13%)	2/8 (25%)		3/8 (38%)	5/8 (63%)
H727-LUC	0/8 (0%)	8/8 (100%)	3/8 (38%)	1/8 (13%)	2/8 (25%)				5/8 (63%)	1/8 (13%)	0/8 (0%)	6/8 (75%)
H1299-LUC	0/8 (0%)	0/8 (0%)	0/8 (0%)	2/8 (25%)		3/8 (38%)					0/8 (0%)	0/8 (0%)
SK-MES-1-LUC	0/8 (0%)	0/8 (0%)	0/8 (0%)	2/8 (25%)	2/8 (25%)	1/8 (13%)					1/8 (13%)	1/8 (13%)

[a] Evaluated upon necropsy at sacrifice according to Ethical guidelines

was markedly lower (168 in average) compared to A549-inoculated animals (Fig. 3b). There was a correlation between tumor burden and metastatic area. Thus, similar osteolytic lesions can result from different degrees of tumor burden.

Other metastasis-related pathology

Body weight was examined to monitor signs of cachexia. Bioluminescence detection of H460 cells in long bones and the development of bone metastasis correlated with decreased body weight. Similar signs were detected in A549-inoculated animals with overt tumor burden. In contrast, body weight in mice inoculated with H727 was not altered compared to non-bone metastatic SK-MES-1 bearing animals or non-inoculated mice, even with the presence of prominent tumor lesions (Fig. 3c). More importantly, animals inoculated with H727 cells presented no signs of cachexia at a time when profound osteolytic lesions were detected by X-rays. These data indicate that the induction of cachexia represents an intrinsic feature of each tumor that is highly variable among different histological subtypes (Table 1).

Metastatic genes involved in osteolytic lesions

To explore the mechanisms that could account for the differences in metastasis observed in vivo, we first determined the proliferation rate of these three cell lines. Doubling times for H460, A549 and H727 cells were 19.5 ± 0.8; 23.9 ± 1.8 and 59.6 ± 8.6 h, respectively, which indicated some correlation with the time of latency in the appearance of metastatic lesions in vivo (Fig. 3d, left panel). However, when these cell lines were injected subcutaneously, the growth of H460-derived tumors was associated with in vitro cell growth, whereas H727-derived tumors grew faster than those derived from A549 cells (Fig. 3d, right panel). These findings indicate that cell growth in vivo is highly dependent on the in vivo microenvironment.

Next, we assessed the expression of three cytokines previously associated with osteolytic lesions: MIP-1α, PTHrP, and interleukin (IL)-8 [34, 35]. In conditions that mimicked tumor–stroma interactions by co-culture with murine bone marrow ST-2 cells, higher levels of MIP-1α and PTHrP were found in aggressive H460 cells, whereas IL-8 levels were decreased (Fig. 4a). In contrast, IL-8 levels were increased by cell–cell interactions by ST-2 cells, whereas PTHrP expression levels were unaffected in A549 cells. A slight increase in PTHrP expression was observed by the conditioned medium of ST-2 cells in A549 cells. In more indolent H727 cells, none of the three osteoclastogenic cytokines were stimulated under these

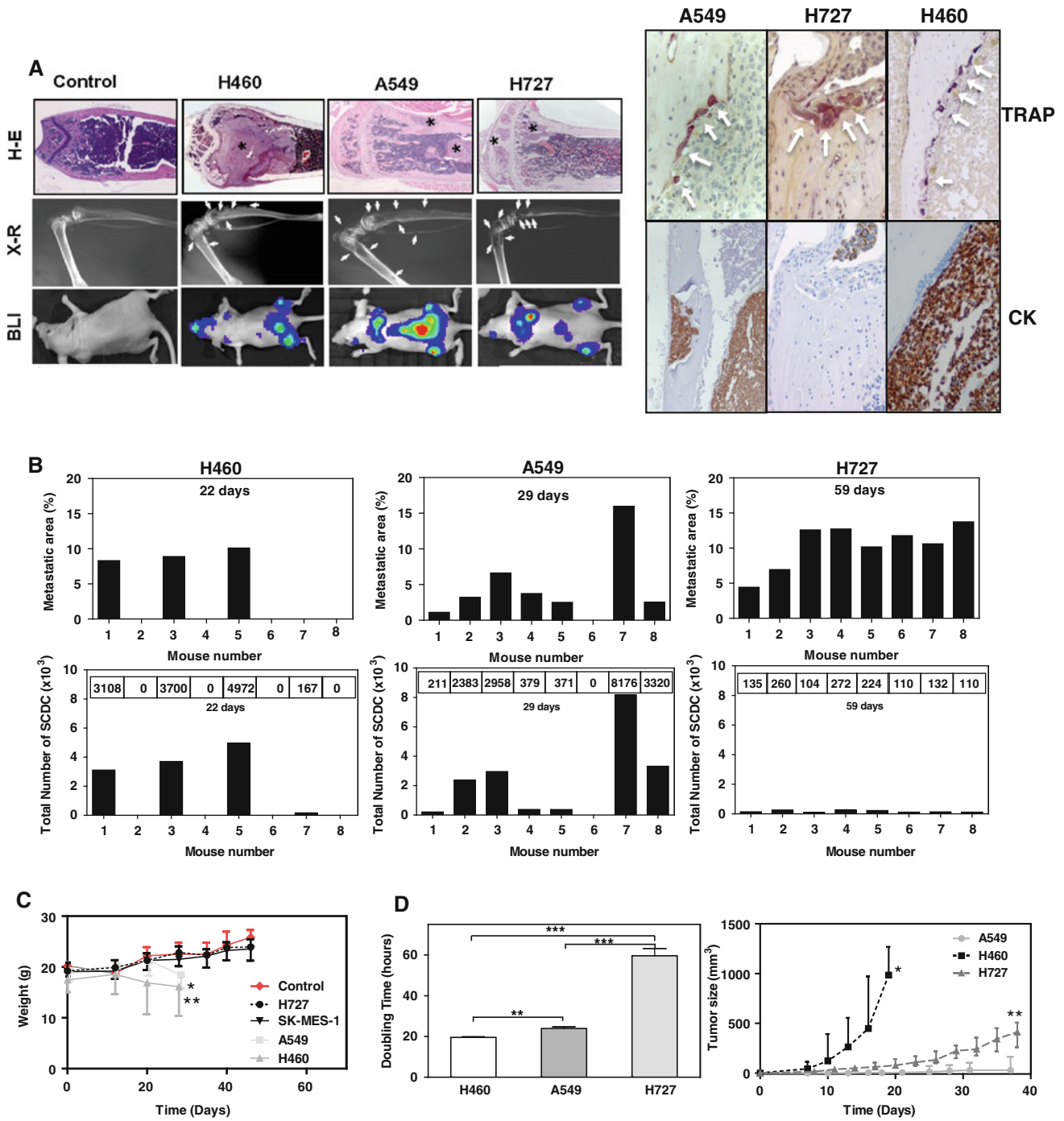

Fig. 3 **a** *Left panel*: Histological (haematoxylin-eosin, H-E), radiographic (X-R) and bioluminescence (BLI) images of bone lesions in femora induced by H460, A549 and H727 cells. "*" denotes the presence of tumor cells. Note the presence of metastatic mass in H460 bearing bone invading cortical bone and marrow cavity, two metastatic focuses in femur at the periosteum and marrow cavity, and epiphyseal and metaphyseal metastases in H727 bearing long bone. *Arrows* indicate the location of osteolytic lesions in X-R images. *Right panel*: serial sections including histochemical detection of osteoclasts (*red staining*) at the tumor–bone interface by TRAP staining and immunohistochemistry using a pan-cytokeratin antibody (CK) to ensure the presence of metastastic cells (*brown*). **b** *Top*: Bone metastatic area in hind limbs of mice i.c. inoculated with H460 (22 days post-inoculation), A549 (29 days post-inoculation), and H727 cells (59 days post-inoculation). *Bottom*: Single cell derived colonies (SCDC) obtained after bone marrow "flushing" of femur and tibiae at these time points. SCDCs were counted in 8 mice inoculated for each cell line. **c** Body weight during metastasis progression after i.c. inoculation of different cell lines (ANOVA followed by Tukey Multiple Comparison Test, $^{**}P < 0.01$; $^{*}P < 0.05$). **d** *Left panel*: Doubling time in vitro for each cell line (Welch test followed by Tamhane multiple comparison). *Right panel*: Tumor growth after subcutaneous injection of each cell line in 6 mice per group (Welch followed by Tamhane multiple comparison test at day 19, $^{*}P < 0.05$ in H460 vs. A549 and H460 vs. H727; Welch test at day 37, $^{**}P < 0.01$ in A549 vs. H727)

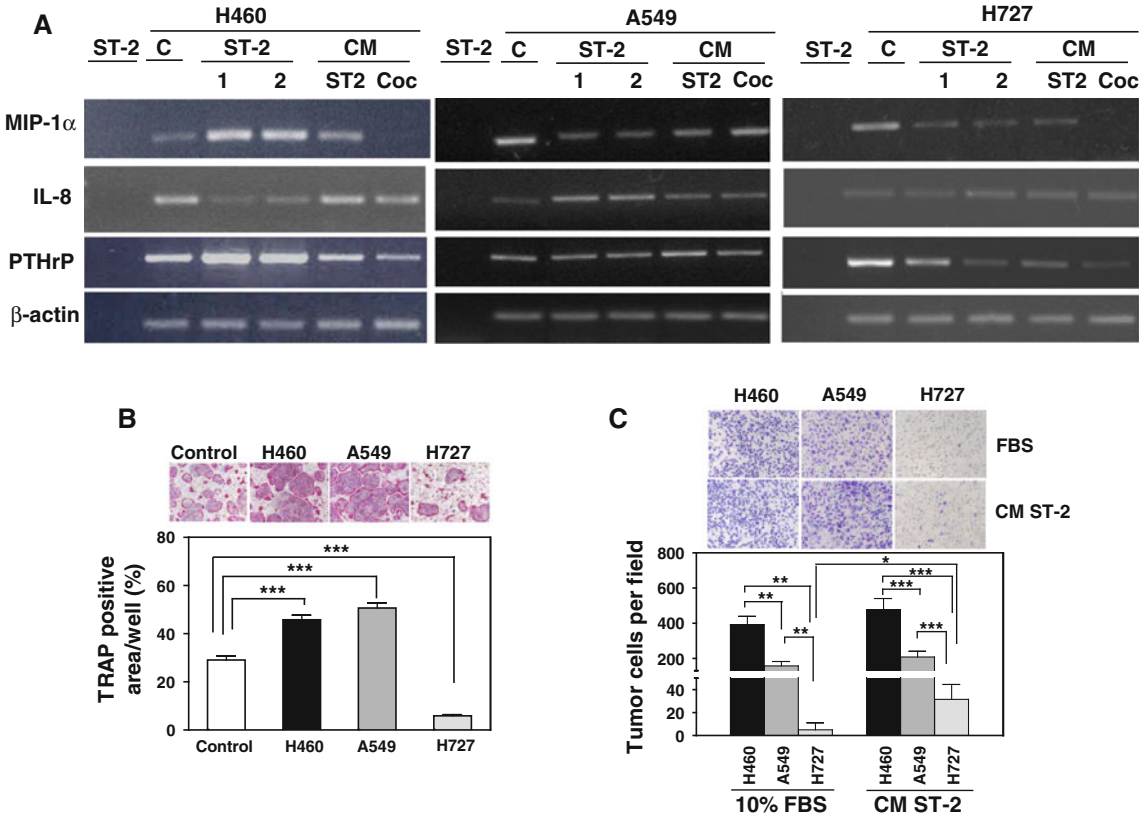

Fig. 4 **a** Semi-quantitative RT-PCR analysis of the expression levels of prosteoclastogenic factors MIP-1α, IL-8 and PTHrP in A549, H460, and H727 cells alone or in coculture with ST-2 cells. Tumor cells were incubated alone with medium (Vehicle, C), in the presence of murine marrow stromal ST-2 cells (1: 10^6 tumor cells; 2: 2×10^6 tumor cells), or with conditioned medium (CM) from ST-2 or the coculture (Coc) for 2 days. Specific human primers were used. **b** In vitro osteoclastogenic assay. Conditioned media from different cell lines was collected and then incubated with murine bone marrow macrophages for 6 days in macrophage colony-stimulating factor (20 ng/ml) and receptor activator of nuclear factor-κB (20 ng/ml)-containing medium. The conditioned medium of A549 and H460 cells induced the highest numbers and robust TRAP-positive multinucleated cells. The experiment was repeated three times with similar results. **c** Chemotactic assay in Boyden chamber using 10% FCS or conditioned medium of ST-2 cells as chemoattractant in the lower compartment after 6 h. Cells were fixed and stained with crystal violet. Twenty fields per well (20×) were quantified using Image Analysis software (ANOVA followed by Tukey Multiple Comparison Test, $***P < 0.001$; $**P < 0.01$, $*P < 0.05$)

experimental conditions (Fig. 4a). These data suggest that expression of these osteoclastogenic cytokines in conditions that mimic tumor–stroma interactions was associated with the latency time in the development of the osteolytic lesions that were observed in vivo.

Osteoclast activity

To investigate whether upregulation of osteoclastogenic factors was correlated with increased osteoclast activity, we determined the ability of secreted factors to stimulate osteoclast formation in an in vitro assay of murine bone marrow macrophages. Conditioned medium from H460 and A549 cells induced high numbers of $TRAP^+$ osteoclasts in vitro compared to control medium. In contrast, H727 conditioned medium did not induce formation of many $TRAP^+$ cells (Fig. 4b). These data were associated with an increase in osteoclastogenic cytokines secreted in vitro. Moreover, these findings in vitro were correlated with the appearance of osteolytic lesions in vivo and a shorter latency time in the development of bone metastasis.

Migration in vitro

We studied the migratory properties of these cell lines in a Boyden chamber assay. Conditioned medium derived from murine ST-2 stromal cells and 10% FCS were used as a chemoattractants. A marked increase in the migration activity of H460 and A549 cells was detected ($P < 0.001$) as compared to H727 cells under both conditions (Fig. 4c). Migration of H727 cells was significantly increased when ST-2 conditioned medium was used as a chemoattractant as compared to 10% FCS ($P < 0.05$). These results suggest that each cell line displays different invasive properties that are associated with the prometastatic activity observed in vivo.

MMP activity

Since tumor–stroma-derived MMPs represent a frequent mechanism that participates in bone matrix degradation, global MMP activity in conditioned medium was assessed by a kinetic fluorescence assay under these conditions. Culture supernatants obtained by co-culture of each cell line with ST-2 cells induced a 1.5- to 3-fold increase in MMP activity, as compared to single cultures using a fluorescence substrate 1 (preferentially cleaved by MMP-3 and MMP-9) (Fig. 5a). Similar results were obtained using a substrate 2 for A549 and H460 cells (preferentially cleaved by MMP-3 and MMP-10). However, induction of MMP activity with this substrate was much lower in H727 co-cultures as compared to the other two cell lines. This activity was abolished by incubation with the global MMP inhibitor GM6001 (Fig. 5a). These findings indicate that metalloproteolytic activity of tumor cell lines is frequently induced in co-culture conditions, although to a different extent.

We characterized the expression levels of MMP-3 and MMP-10 and gelatinases MMP-2 and MMP-9 for each human tumor cell line and mouse ST-2, alone or in co-culture by specific real-time PCR. MMP-10 was undetected in ST-2 cells, whereas MMP-3 was not expressed in tumor cells under any of the conditions tested (data not shown). A differential pattern of MMP increase in co-culture was detected for each tumor cell line. Although MMP-10 did not increase in A549 cells, in co-culture, MMP-10 expression slightly increased in H460 cells and more markedly in H727 cells (Fig. 5b). Tumor expression levels of MMP-2 and MMP-9 did not increase under co-culture conditions in H460 and A549 cells, whereas robust induction for these two gelatinases was found in H727 cells (Fig. 5b). Basal levels of stromal expression of MMP-3 were undetected, whereas cell–cell interactions of tumor cells with ST-2 cells led to an increase in stromal MMP-3 expression levels with all cell lines. This effect was detected for stromal gelatinases in all cases except for MMP-2 in H727 co-cultures (Fig. 5c). Stromal MMP-3 expression levels induced by tumor cell contacts correlated with the MMP activity observed with substrate 2 (Fig. 5a). Taken together, these data indicate that each tumor cell line induces a different expression profile of MMPs, in the tumor and stromal cells upon tumor–stromal interactions.

Discussion

We have comparatively characterized three in vivo models of lung cancer metastasis from different histological lung cancer subtypes of NSCLC, which gave rise to selective, reproducible and rapid osseous metastasis. The variable expression of osteoclastogenic cytokines, and MMP activity, modulated by stroma highly influenced the in vivo development of osteolytic bone metastasis. Thus, this platform could be a useful tool to dissect the modulatory effects and signaling cascades directed by the bone microenvironment during osseous colonization, as well as the molecular mechanisms involved in tissue tropism. Despite a high degree of similarity, their mechanisms of growth and colonization in the osseous microenvironment remained highly divergent.

Several in vitro findings support this contention. For instance, chemotactic ability induced by stromal cells widely varied among different subtypes. This effect might be relevant in early events of metastatic homing. Of note, chemoattraction of H727 cells was more effective in the presence of conditioned medium of ST-2 cells. This is consistent with the selective expression of CXCR4 chemokine and its ligand in these cells, as compared to A549 and H460 cells (data not shown). In addition, upregulation of osteoclastogenic factors in H460 and A549 cells in conditions that mimicked tumor–stroma interactions was associated with increased osteoclastogenic activity. In these conditions, none of these factors were altered in H727 cells. Despite the limitation of this assay, high osteoclast formation induced by H460 and A549 cells could contribute in vivo to a short latency period and severity of bone colonization. We postulate that this mechanism could prevail in early stages of colonization when tumor-derived factors such as PTHrP, IL-8, MIP-1α or others could facilitate the progressive induction of high numbers of osteoclasts, which promotes initial metastatic expansion. Indeed, delay in the development of metastatic lesions has been shown by inhibition of these cytokines [11].

Furthermore, in conditions that mimicked tumor–stromal interactions, our functional dissection of MMP activity revealed different patterns of tumor–stromal MMP expression profile. However, the strong increase in MMP expression at the stromal component in all co-cultures support a role for the microenvironment in the development of bone lesions. High MMP-3 expression levels were detected in stromal cells upon interaction with A549 and H460 cells as compared to H727 cells, whereas levels were undetected under basal conditions. In contrast, basal levels of MMP-9 in H727 and ST-2 cells were strongly stimulated in co-culture in comparison to those in A549 and H460 cells. Thus, besides the overt MMP-9 expression in tumor and stromal cells in co-culture, its activity might not be germane in this context. This finding is consistent with the irrelevant contribution of MMP-9 to the development of osteolytic lesions in other models of bone metastasis [36]. Nevertheless, our in vitro co-culture system does not fully reconstitute the complexity of the tumor–bone

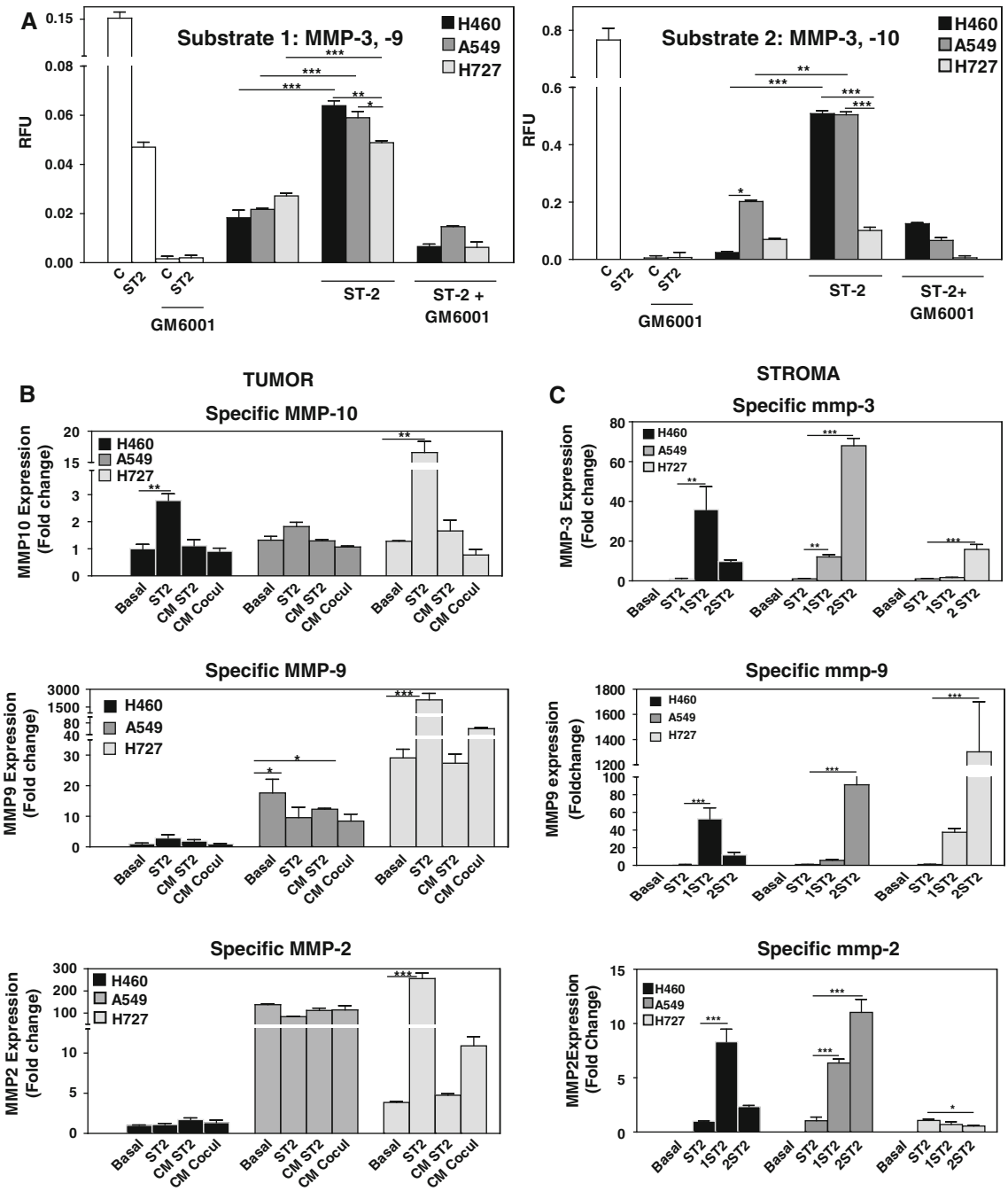

Fig. 5 **a** Global MMP activity in the serum-free conditioned medium of different cell lines alone or in coculture with ST-2 cells assessed by digestion of fluorogenic substrates. Inhibition of MMP activity was performed with a global MMP inhibitor, GM6001. The experiment was repeated three times with similar results. *RFU* relative fluorescence units. (Bonferroni's test). **b** Relative expression of MMP-2, -9 and -10 by real time RT-PCR using specific human primers. Analysis was performed in cells cultured alone with regular medium (Basal), incubated with conditioned medium (CM) from ST-2 or from the coculture (CM Cocul), and in coculture with ST-2 cells (ST2). Human GAPDH was used as endogenous control. **c** Similarly, stromal derived MMP-2, -3 and -9 was assessed in ST-2 cells cultured alone or cocultured with one (1ST-2) or two million (2ST-2) tumor cells using murine primers. Mouse gapdh was used as endogenous control. Represented data at **b** and **c** as mean ± SD (Bonferroni's multiple comparison test)

microenvironment in vivo, where other cells and/or secreted enzymes could potentially contribute to the extracellular proteolytic activity. In this regard, we have recently shown that ADAM8 (a disintegrin and metalloprotease domain) isoforms contribute to the aggressive bone colonization of lung cancer [25]. Moreover the use of a broad-spectrum inhibitor of MMP and ADAM activities markedly attenuates the development of

metastatic lesions [12]. Based on these findings, elucidation of whether any single proteolytic activity could have an indispensable role in bone metastatic progression remains to be addressed.

Effects mediated by the stromal microenvironment were also highly relevant in vivo. The fact that subcutaneous growth did not correlate with in vitro cell growth kinetics, underscores the requirement of microenvironmental cues for proper tumor growth and colonization. Moreover, the distinct patterns of tumor growth between A549 and H727 cells observed in osseous versus subcutaneous locations emphasizes the in vivo requirements imposed by different tumor microenvironments. It remains to be addressed whether similar in vitro MMP and osteoclastogenic activities, exacerbated by tumor–stromal interactions could also strongly influence in vivo osseous colonization.

In addition to differences in colonization, other factors including bone homing should account for the distinct pattern of metastasis development. In our models, bone homing activity was suggested by the consistent location of lesions. The similarity of the sites where metastases developed in the three models argued in favor of a common mechanism by which physical constraints imposed by the microvasculature or specific tumor endothelial/stromal engagement could allow arrest and survival. We have recently shown that in vivo blockade of platelet-derived growth factor receptor (PDGFR) signaling in bone marrow stroma profoundly alters tumor homing in different models of lung cancer bone metastasis [37]. These findings support the relevance of host–tumor interactions for permissive bone homing in vivo.

The propensity of the selected cells to form bone lesions also suggests the unique and favorable conditions that are imposed by the osseous microenvironment. Indeed, the skeleton is a major reservoir of growth factors including TGF-β and insulin-like growth factor. TGF-β has been shown to be crucial in fuelling the osteolytic lesions by upregulating several of the osteoclastogenic genes as shown for breast [8, 38] and renal cell [9] carcinoma. We have recently shown that in vivo TGF-β blockade in an H460 cell model results in inhibition of bone metastatic colonization [12]. However, no effects were found using the same strategy in A549 and H727 cells (data not shown), which suggests that TGF-β-independent mechanisms drive osseous deleterious lesions. Thus, the involvement of TGF-β as a common mechanism in lung cancer bone metastasis remains highly dependent upon each histological subtype.

In the A549 and H460 xenografts, the appearance of cachexia during metastasis development closely mimicked disease progression in humans. With regard to the mechanisms of cachexia, it has been suggested that one or several tumor-released factors, such as PTHrP, could be involved in energy wasting and body weight regulation [39]. Other factors have been shown to mediate cachexia, including tumor necrosis factor-α, IL-6 and IL-1 [40], many of which are highly regulated by tumor–stromal interactions in the bone microenvironment. A recent study has shown the importance of a signaling pathway mediated through activin receptor type IIB, a member of the TGF-β receptor family, for regulating muscle atrophy by increasing the ubiquitin–proteasome proteolytic pathway [41]. In addition, other signaling pathways could be relevant in this regard. For instance, blockade of PDGFR signaling in bone marrow stroma delayed the appearance of cachexia in lung cancer bone metastasis [37].

Given the similarity with human pathology, these models could allow the identification of key target molecules and the screening of new therapeutic modalities for prevention of bone metastasis. Future studies will be developed to identify key regulatory genes involved in this process.

Acknowledgments We are grateful to Dr. Pina for his valuable help assessing radiographs and the members of the Morphology Core facility and Animal Core Facilities. This work was supported by "UTE project FIMA" agreement, and RTICC C03/10, FIT-090100-2005-46, PI042284, PI070031, SAF-2009-11280 (to FL), Royo Foundation (SV), FPU (DL-R and KV), and Basque Government (IA). FL is also supported by funds from the I3 Program, "La Caixa Foundation", and grants 67/2005, 09/2009 from the Government of Navarra. There are no conflicts of interest to disclose.

References

1. Jemal A, Tiwari RC, Murray T, Ghafoor A, Samuels A, Ward E, Feuer EJ, Thun MJ (2004) Cancer statistics, 2004. CA Cancer J Clin 54:8–29
2. Tuveson DA, Jacks T (1999) Modeling human lung cancer in mice: similarities and shortcomings. Oncogene 18:5318–5324
3. Ginsberg RJ, Kris MG, Armstrong JG (2001) Non-small cell lung cancer. Lippencott Williams and Wilkins, Philadelphia, PA
4. Coleman RE (1997) Skeletal complications of malignancy. Cancer 80:1588–1594
5. Delea T, Langer C, McKiernan J, Liss M, Edelsberg J, Brandman J, Sung J, Raut M, Oster G (2004) The cost of treatment of skeletal-related events in patients with bone metastases from lung cancer. Oncology 67:390–396
6. Fidler IJ (2003) The pathogenesis of cancer metastasis: the 'seed and soil' hypothesis revisited. Nat Rev Cancer 3:453–458
7. Nguyen DX, Massague J (2007) Genetic determinants of cancer metastasis. Nat Rev Genet 8:341–352
8. Kakonen SM, Selander KS, Chirgwin JM, Yin JJ, Burns S, Rankin WA, Grubbs BG, Dallas M, Cui Y, Guise TA (2002) Transforming growth factor-beta stimulates parathyroid hormone-related protein and osteolytic metastases via Smad and mitogen-activated protein kinase signaling pathways. J Biol Chem 277:24571–24578
9. Kominsky SL, Doucet M, Brady K, Weber KL (2007) TGF-beta promotes the establishment of renal cell carcinoma bone metastasis. J Bone Miner Res 22:37–44
10. Yin JJ, Selander K, Chirgwin JM, Dallas M, Grubbs BG, Wieser R, Massague J, Mundy GR, Guise TA (1999) TGF-beta signaling

blockade inhibits PTHrP secretion by breast cancer cells and bone metastases development. J Clin Invest 103:197–206
11. Guise TA, Yin JJ, Taylor SD, Kumagai Y, Dallas M, Boyce BF, Yoneda T, Mundy GR (1996) Evidence for a causal role of parathyroid hormone-related protein in the pathogenesis of human breast cancer-mediated osteolysis. J Clin Invest 98: 1544–1549
12. Vicent S, Luis-Ravelo D, Anton I, Garcia-Tunon I, Borras-Cuesta F, Dotor J, De Las Rivas J, Lecanda F (2008) A novel lung cancer signature mediates metastatic bone colonization by a dual mechanism. Cancer Res 68:2275–2285
13. Chen JJ, Peck K, Hong TM, Yang SC, Sher YP, Shih JY, Wu R, Cheng JL, Roffler SR, Wu CW et al (2001) Global analysis of gene expression in invasion by a lung cancer model. Cancer Res 61:5223–5230
14. Onn A, Isobe T, Itasaka S, Wu W, O'Reilly MS, Ki Hong W, Fidler IJ, Herbst RS (2003) Development of an orthotopic model to study the biology and therapy of primary human lung cancer in nude mice. Clin Cancer Res 9:5532–5539
15. Kakiuchi S, Daigo Y, Tsunoda T, Yano S, Sone S, Nakamura Y (2003) Genome-wide analysis of organ-preferential metastasis of human small cell lung cancer in mice. Mol Cancer Res 1:485–499
16. Liu J, Blackhall F, Seiden-Long I, Jurisica I, Navab R, Liu N, Radulovich N, Wigle D, Sultan M, Hu J et al (2004) Modeling of lung cancer by an orthotopically growing H460SM variant cell line reveals novel candidate genes for systemic metastasis. Oncogene 23:6316–6324
17. Khanna C, Hunter K (2005) Modeling metastasis in vivo. Carcinogenesis 26:513–523
18. Yamaura T, Murakami K, Doki Y, Sugiyama S, Misaki T, Yamada Y, Saiki I (2000) Solitary lung tumors and their spontaneous metastasis in athymic nude mice orthotopically implanted with human non-small cell lung cancer. Neoplasia 2:315–324
19. Yang M, Hasegawa S, Jiang P, Wang X, Tan Y, Chishima T, Shimada H, Moossa AR, Hoffman RM (1998) Widespread skeletal metastatic potential of human lung cancer revealed by green fluorescent protein expression. Cancer Res 58:4217–4221
20. Zheng S, El-Naggar AK, Kim ES, Kurie JM, Lozano G (2007) A genetic mouse model for metastatic lung cancer with gender differences in survival. Oncogene 26:6896–6904
21. Jackson EL, Olive KP, Tuveson DA, Bronson R, Crowley D, Brown M, Jacks T (2005) The differential effects of mutant p53 alleles on advanced murine lung cancer. Cancer Res 65: 10280–10288
22. Carney DN, Gazdar AF, Bepler G, Guccion JG, Marangos PJ, Moody TW, Zweig MH, Minna JD (1985) Establishment and identification of small cell lung cancer cell lines having classic and variant features. Cancer Res 45:2913–2923
23. Mitsudomi T, Steinberg SM, Nau MM, Carbone D, D'Amico D, Bodner S, Oie HK, Linnoila RI, Mulshine JL, Minna JD et al (1992) p53 gene mutations in non-small-cell lung cancer cell lines and their correlation with the presence of ras mutations and clinical features. Oncogene 7:171–180
24. Mitsudomi T, Viallet J, Mulshine JL, Linnoila RI, Minna JD, Gazdar AF (1991) Mutations of ras genes distinguish a subset of non-small-cell lung cancer cell lines from small-cell lung cancer cell lines. Oncogene 6:1353–1362
25. Hernandez I, Moreno JL, Zandueta C, Montuenga L, Lecanda F (2010) Novel alternatively spliced ADAM8 isoforms contribute to the aggressive bone metastatic phenotype of lung cancer. Oncogene 29:3758–3769
26. Eltarhouny SA, Elsawy WH, Radpour R, Hahn S, Holzgreve W, Zhong XY (2008) Genes controlling spread of breast cancer to lung "gang of 4". Exp Oncol 30:91–95
27. Tester AM, Waltham M, Oh SJ, Bae SN, Bills MM, Walker EC, Kern FG, Stetler-Stevenson WG, Lippman ME, Thompson EW (2004) Pro-matrix metalloproteinase-2 transfection increases orthotopic primary growth and experimental metastasis of MDA-MB-231 human breast cancer cells in nude mice. Cancer Res 64:652–658
28. Zhao Q, Guo X, Nash GB, Stone PC, Hilkens J, Rhodes JM, Yu LG (2009) Circulating galectin-3 promotes metastasis by modifying MUC1 localization on cancer cell surface. Cancer Res 69:6799–6806
29. Roodman GD (2001) Biology of osteoclast activation in cancer. J Clin Oncol 19:3562–3571
30. Han JH, Choi SJ, Kurihara N, Koide M, Oba Y, Roodman GD (2001) Macrophage inflammatory protein-1alpha is an osteoclastogenic factor in myeloma that is independent of receptor activator of nuclear factor kappaB ligand. Blood 97:3349–3353
31. Iguchi H, Tanaka S, Ozawa Y, Kashiwakuma T, Kimura T, Hiraga T, Ozawa H, Kono A (1996) An experimental model of bone metastasis by human lung cancer cells: the role of parathyroid hormone-related protein in bone metastasis. Cancer Res 56:4040–4043
32. Kang Y, Siegel PM, Shu W, Drobnjak M, Kakonen SM, Cordon-Cardo C, Guise TA, Massague J (2003) A multigenic program mediating breast cancer metastasis to bone. Cancer Cell 3: 537–549
33. Asou Y, Rittling SR, Yoshitake H, Tsuji K, Shinomiya K, Nifuji A, Denhardt DT, Noda M (2001) Osteopontin facilitates angiogenesis, accumulation of osteoclasts, and resorption in ectopic bone. Endocrinology 142:1325–1332
34. Bendre MS, Gaddy-Kurten D, Mon-Foote T, Akel NS, Skinner RA, Nicholas RW, Suva LJ (2002) Expression of interleukin 8 and not parathyroid hormone-related protein by human breast cancer cells correlates with bone metastasis in vivo. Cancer Res 62:5571–5579
35. Bendre MS, Margulies AG, Walser B, Akel NS, Bhattacharrya S, Skinner RA, Swain F, Ramani V, Mohammad KS, Wessner LL et al (2005) Tumor-derived interleukin-8 stimulates osteolysis independent of the receptor activator of nuclear factor-kappaB ligand pathway. Cancer Res 65:11001–11009
36. Thiolloy S, Halpern J, Holt GE, Schwartz HS, Mundy GR, Matrisian LM, Lynch CC (2009) Osteoclast-derived matrix metalloproteinase-7, but not matrix metalloproteinase-9, contributes to tumor-induced osteolysis. Cancer Res 69:6747–6755
37. Catena R, Luis-Ravelo D, Anton I, Zandueta C, Salazar-Colocho P, Larzabal L, Calvo A, Lecanda F (2011) PDGFR signaling blockade in marrow stroma impairs lung cancer bone metastasis. Cancer Res 71:164–174
38. Yin JJ, Pollock CB, Kelly K, Kakonen SM, Selander KS, Chirgwin JM, Burns S, Rankin WA, Grubbs BG, Dallas M et al (2005) Mechanisms of cancer metastasis to the bone. Cell Res 15:57–62
39. Iguchi H, Onuma E, Sato K, Ogata E (2001) Involvement of parathyroid hormone-related protein in experimental cachexia induced by a human lung cancer-derived cell line established from a bone metastasis specimen. Int J Cancer 94:24–27
40. Tisdale MJ (2002) Cachexia in cancer patients. Nat Rev Cancer 2:862–871
41. Zhou X, Wang JL, Lu J, Song Y, Kwak KS, Jiao Q, Rosenfeld R, Chen Q, Boone T, Simonet WS et al (2011) Reversal of cancer cachexia and muscle wasting by ActRIIB antagonism leads to prolonged survival. Cell 142:531–543